Response to Anonymous Referee #1:

We would like to thank the referee for their comments and suggestions. Their comments have allowed us to improve the manuscript and correct errors in the text. In the following we have reproduced the referee's comments in italics and provided our response in bold text.

Where necessary we provide the text we have used in the revised manuscript in plain text.

Referee: *"First of all, as the paper is mainly based on finding the source of errors associated with the Full Correlation Analysis applied to MF radar, I would have liked to see this method better explained. Although this method is explained in full detail in Briggs et al. (1984), this paper is quite difficult to find and it would rather be useful for a reader to have at least the basic principles of such a method reminded in the present paper. As the paper is not too long, I do not think it would be much of a problem to add a section about this method."*

We have inserted a basic description of the Full Correlation Analysis as an appendix and referred to it within the main body of the paper (copied at the end of this response). We felt that inserting a section into the main body of the paper would disrupt the flow. We hope this is acceptable.

Referee: *"Second, one of the central figure of the paper is missing: that is Figure 9. As this figure is supposed to fully confirm that there is a strong correlation between axial ratio and both number of outliers and hourly variance and thus that the radar data quality are the cause of the large wind values, I would really like to see this figure before accepting this paper."*

Our apologies over the missing figure 9, when we first uploaded the manuscript it was missing, the editorial staff quickly informed us and we uploaded a new copy (which is downloadable from the site as the discussion paper); however clearly you were sent the original. The figure and caption are reproduced below.

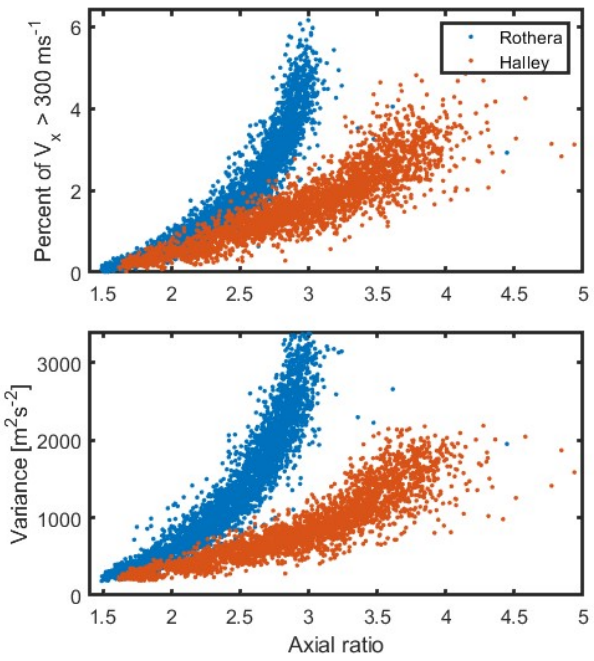

Figure 9. The relationship between axial ratio and (a) outliers and (b) hourly variance of the zonal wind. Each point represents a different hour, month and altitude, to isolate the effect of differing error levels. Only altitudes over 80 km are shown. Meridonal winds show substantially the same relationship, with slightly smaller variances.

Referee: *"Third, I would like to see explained why the correlation analysis made with respect to solar insolation and geomagnetic activity are only performed with zonal winds. This is not explained anywhere and sometimes, it is not even clear if this is only zonal winds or combined zonal and meridional wind, which are presented, especially in figure 10 where it is not stated neither in the captions nor in the associated text. If for example, meridional winds naturally show a smaller signal variance then it is worth stating it."*

Thank you for pointing this out, this was a significant oversight on my part. We have included a more detailed description of the analysis in the manuscript and made sure that we indicate which data are being presented in each case! In actual fact we did the analysis with both the zonal and meridional winds and found similar results for both. We had opted to show just the zonal winds to limit the size of the plots; however following the reviewer's comments we have included both wind directions in some of the plots and made sure we reference both in the text of the manuscript. Altered plots are provided below:

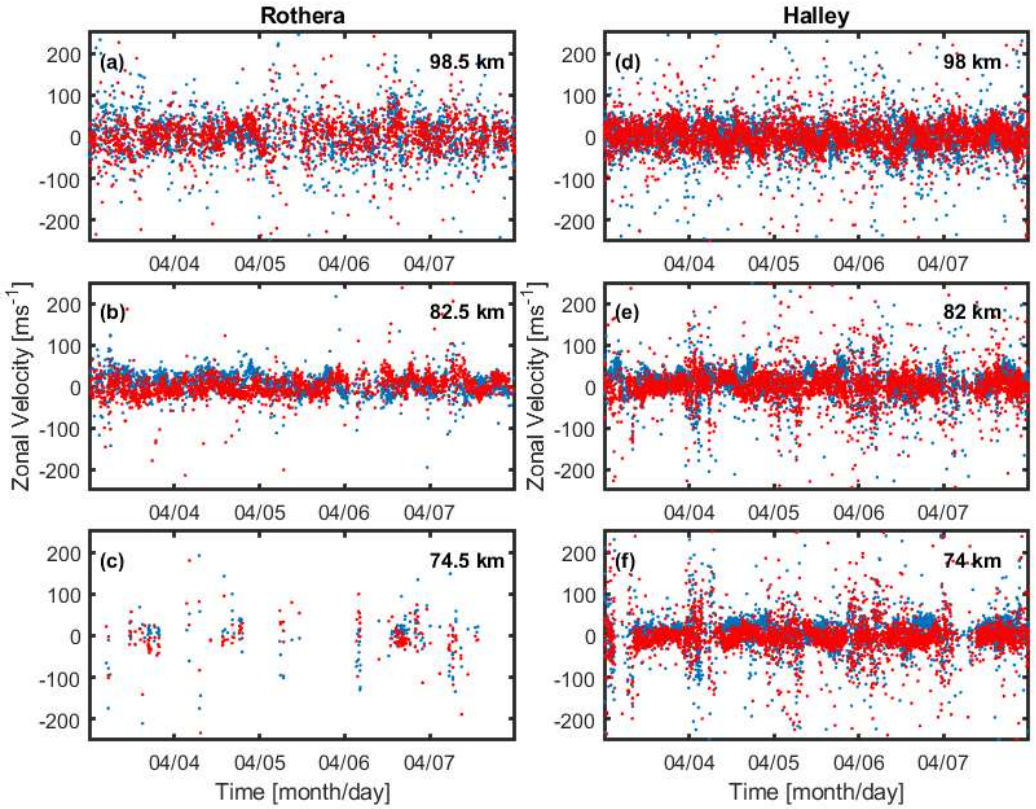

Figure 2. Sample data from the Rothera (left) and Halley (right) radars for three comparable heights from 3-7 April 2013. Blue dots represent zonal winds, red dots represent meridional winds. Large variability can be seen in each plot. At the lowest altitude, Rothera (c) is experiencing a loss of scatter due to a weaker (than Halley (f)) returned signal.

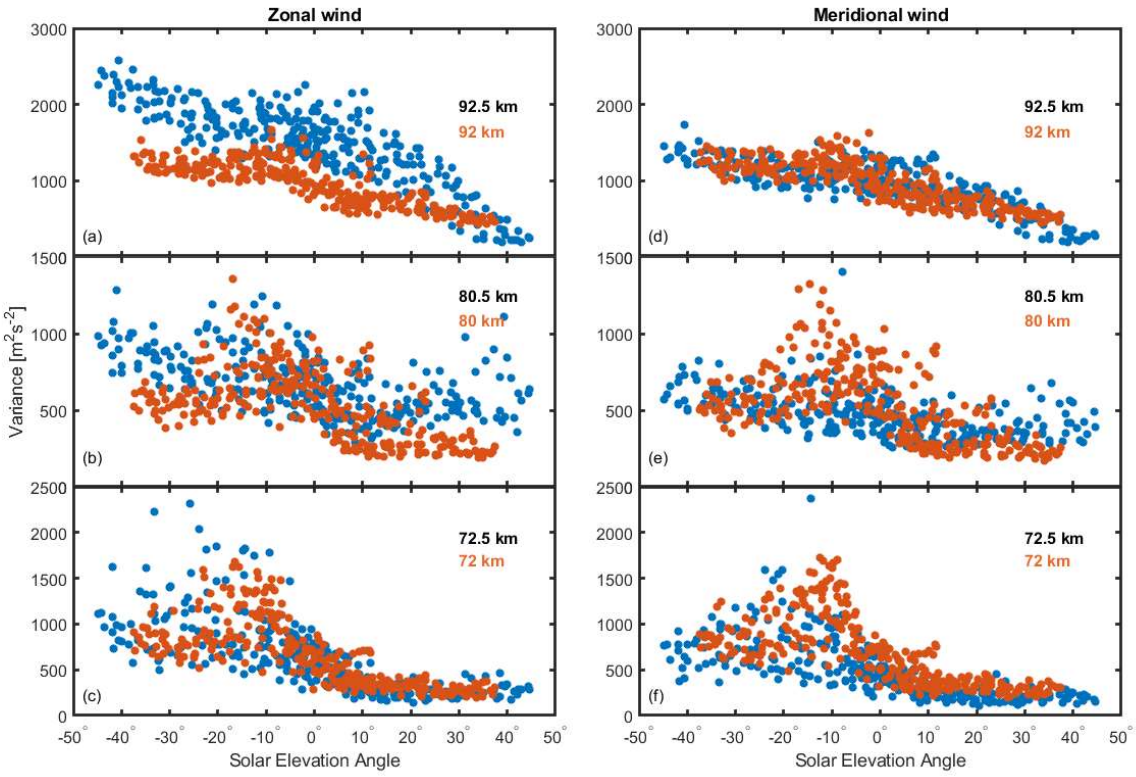

Figure 8. Zonal (left) and meridional (right) wind variance from the Rothera (blue) and Halley (Orange) radar for three altitudes, as a function of solar elevation angle.

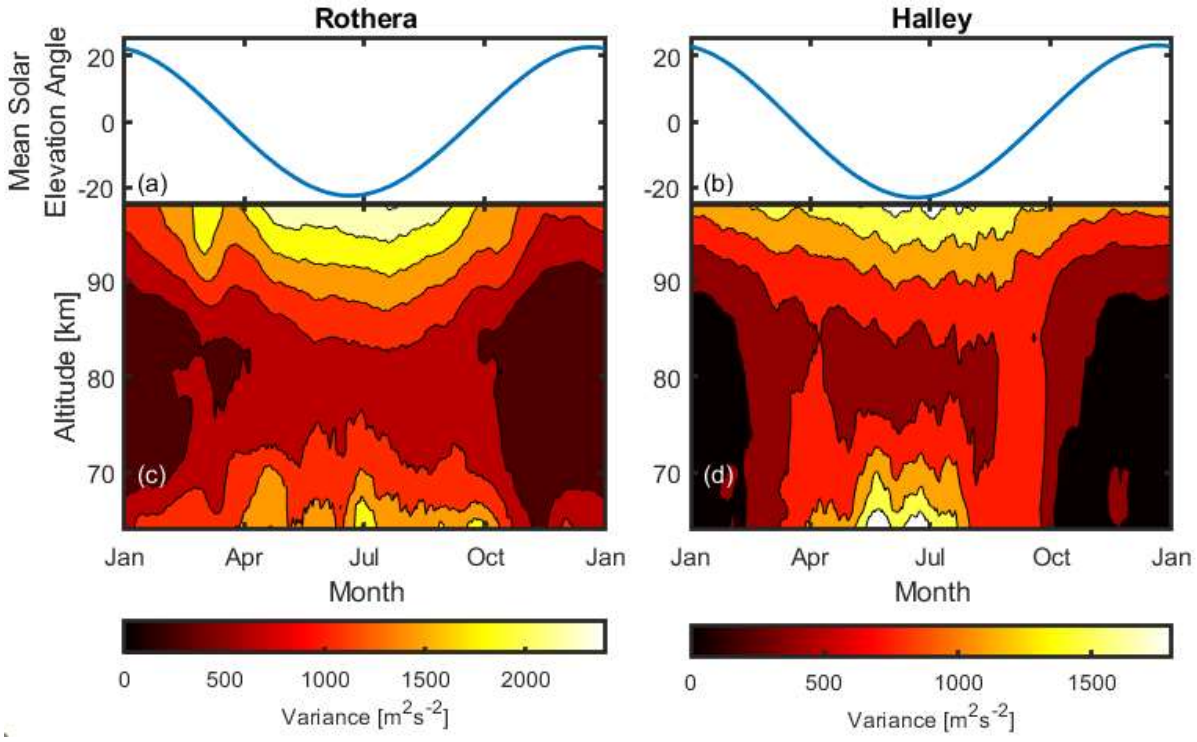

Figure 10. Trends in variance over the course of the year at Rothera (c) and Halley (d) with the daily mean angle of the sun above the horizon ((a) and (b)). Mean variances were calculated for each day and the result smoothed using a 15-day running mean. Note the difference in colour scale between the two plots.

Referee: *"Finally, I would like to see better explanation for Figure 11. Indeed, as the AE index is a measure of the geomagnetic activity in the Northern hemisphere while the MF radars data analyzed in this paper are in the Southern Hemisphere, it will be good to better describe the seasonal correlation, in particular for which seasons correspond the maxima and the minima of the correlation coefficients and to explain physically these and minima."*

The referee is correct that the AE index is derived from northern magnetic stations. Furthermore it is a global scale (or perhaps half-global scale) measurement since it is averaged across those stations spread in longitude. Its purpose is to provide an indication of geomagnetic activity – driven primarily by the substorm cycle. Substorms are global phenomena and although there can be quite drastic differences in the local scale structure, magnitude and positioning of auroral forms (and the underlying magnetic topology), between the poles, in a statistical sense the AE index will still be representative of geomagnetic activity in the south. We have updated the text to improve the explanation, and we have modified old figures 11 and 12 into a single figure. We have also altered to analysis slightly to concentrate on the annual cycle and the effects around the zero lag,

"To probe this relationship the Auroral Electroject (AE) index is used as a measure of geomagnetic activity. This index is derived from geomagnetic variations in the horizontal component of the magnetic field observed by 10 to 13 stations in the auroral zone in the northern hemisphere. The AE index is the difference between the largest and smallest values detected by these stations, produced at 1-minute resolution. It responds most strongly to the substorm cycle, where energy is loaded in the magnetotail from the solar wind, and then released earthward generating the auroral electroject and auroral displays. Although there can be quite drastic differences in the local scale structure, magnitude and positioning of auroral forms (and the underlying magnetic topology), between the poles, in a statistical sense the AE index will still be representative of geomagnetic activity in the south.

Figure 11, panel (a), shows the cross correlation between the hourly maximum AE index and the hourly zonal wind variance measured at Halley at three altitudes: 90 km, 80 km and 70 km the meridional winds show the same results). Each of the data sets have been normalized such that their autocorrelations equal one at the zero lag and lie between 1and -1. At each altitude there is an annual cycle in the correlation, though the value of the coefficient is relatively small (<0.2). This cycle is due to the seasonal variations of both the variance and the AE index; the variability of the AE index is driven by changes in solar wind activity, but the coupling to Earth's magnetic environment has a seasonal component known as the Russell-McPherron effect, whereby the coupling maximises around the equinoxes. Figure 10 illustrated that there is a seasonal pattern in the variance, which matches the level of solar illumination.. Panel (b) of fig. 11 shows the cross correlation for 40 days around the zero lag; there is a clear positive correlation at the zero lag for 90 km and a smaller negative correlation for 70 km. Variances at 80 km show little evidence of a relationship with geomagnetic activity.

These observations can be explained as follows: During periods of high geomagnetic activity, there is an influx of high-energy particles into the mesosphere (e.g. Brasseur and Solomon, 2005). This means that at lower altitudes, where there is normally very little ionisation, the ionisation levels increase, and partial reflection of radio waves is stronger. As we have already seen, measured wind variance is related to the scatter quality, so an increased scatter quality corresponds to a lower measured variance at 60 km.

Increased ionisation levels at the lower altitudes also have the effect of absorbing radio waves that pass through, meaning that the quality of signal for radio waves partially reflected at higher altitudes is diminished. Thus, we see the inverse effect for data from 90 km: periods with increased geomagnetic activity correspond to an in- crease in measured variance at higher altitudes, as the amount of data decreases. The correlations seen at 70 and 90 km decay with lag times of about 5-10 days, suggesting that this is the time scale over which the ionisation levels return to normal after a geomagnetic event. This would be in line with studies of energetic precipitation driven by solar wind transients such as high speed solar wind streams (e.g. Kavanagh et al., 2012). This reflects the pattern of SNR seen in (Kavanagh et al 2018) at Rothera in response to increased precipitation where there is a reduction in data at high altitudes due to signal loss and a gain in data at the lower altitudes. This hints at an underlying relationship between variance and data quality (in terms of the amount of data seen)."

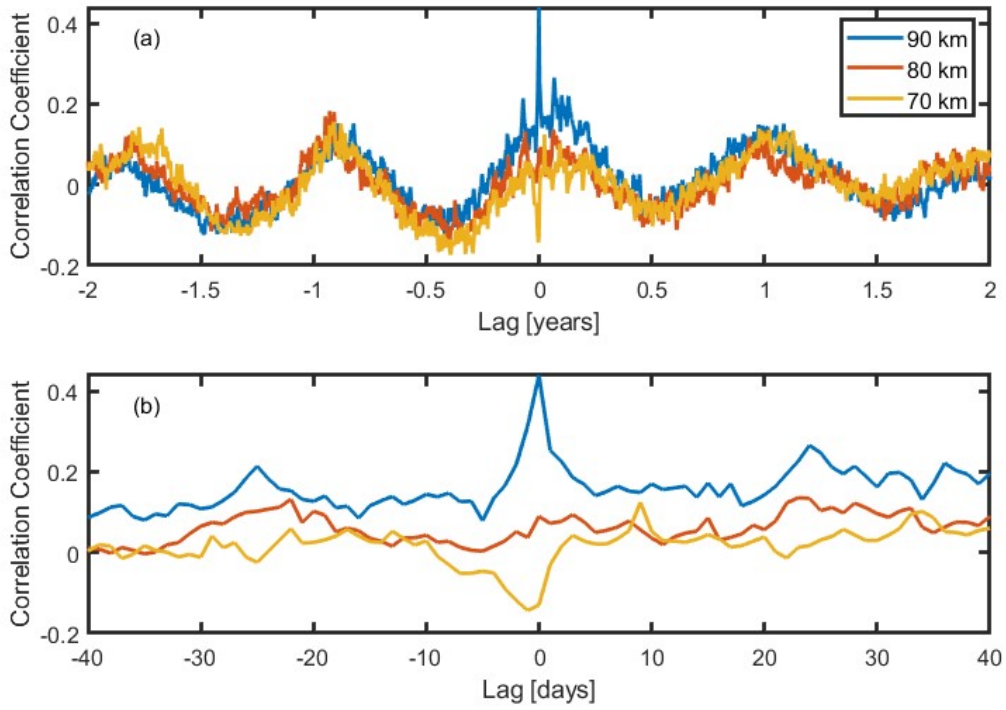

Figure 11. Correlation coefficients between maximum AE index in each hour and zonal wind variance observed at Halley shown at a range of lag times. Panel (a) shows the long term correlation: the sinusoidal nature of the correlation shows a seasonal cycle. Peaks are seen at zero lag at 70 and 90 km, suggesting a relationship beyond the seasonal variations. In panel (b) the central peaks are shown A distinct correlation at zero lag is seen for some altitudes, positive at 90 km and negative at 70 km. The same result is found for meridional winds.

I would like to add that following the results of this paper, it is my intention to have a student project examining the response of the radar to local magnetic variations in more detail. But that is an additional significant amount of work designed to build upon this work and as such is beyond the scope of this paper.

Referee: "Other question: On Figure 7, I am really surprised that the solar elevation angle with respect to local time is so different between April and October whereas these two months are very close to equinoxes. Are the authors sure of their calculation? "

We have checked the calculations and are happy with them. To reassure the referee we have included some additional plots below. A factor to remember is that the plots represent averages across a whole month and so we are mixing data that is quite some time away from equinox in both cases

Figure R1.1 (a) shows the monthly average of the solar elevation angle as in Figure 7 of the manuscript, except that April and October have been replaced with the equinox months of March (red) and September (purple). Note that the solar elevation angles are much closer. It is worth noting the much more similar variance values for those two periods displayed in (b). Figure R1.2 is the same but instead of monthly averages we have averaged 28days surrounding the equinoxes; in this case the red and purple lines almost completely overlie one another, and again the corresponding variance curves are much more similar

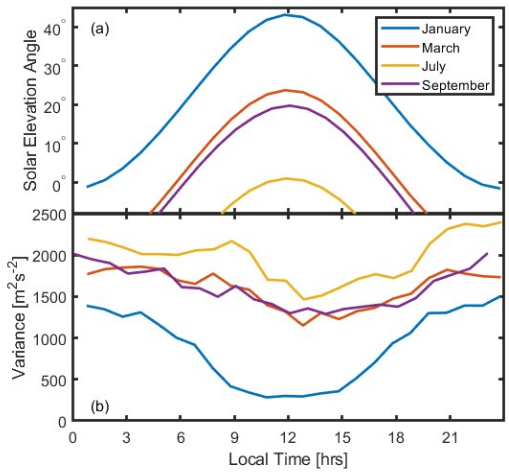

Fig. R1.1 As figure7 in the discussion paper but using March and September instead of April and October.

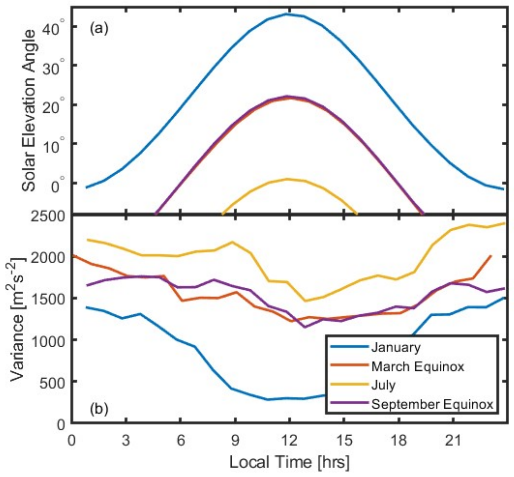

Fig R1.2 As figure R1.1 but with 28 day averages centred around the equinoxes.

Referee: *Line 99: "for Rothera, the diurnal tide maximizes in Winter whilst the semi-diurnal peaks in winter": I wonder if there is not a problem in the seasons listed in this sentence, is it really always winter?*

Line 99: the reviewer is quite correct the first 'winter' should have been 'summer'

Line 134: "The data in fig. 3..." should be replaced by "The data in fig. 4..."

Line 134: corrected.

Appendix

Full Correlation Analysis (FCA) is a technique developed in the late 1980s at Adelaide University to obtain the bulk motion of a generally anisotropic, time-evolving pattern probed by at least three sensors continuously in time. In the case of spaced-antenna radar observation of atmospheric winds, the pattern is that of radio wave reflections from the atmosphere, and the sensors are antennae recording the reflected radio wave signal.

In general, this method can use (with increasing levels of redundancy) an arbitrary number of sensors; here we show the simplest case, with just three antennae arranged in an L- shape. This is a reproduction of the algorithm as presented in Briggs [6].

The setup is shown in Figure 13. Three sensors, S0, S1, and S2 are located along the orthogonal directions and each records the pattern strength at their local position continuously as a function of time. From these recorded signals f (x, y, t), correlation functions with lag time τ, and across distances ξ and η in the x- and y-directions are calculated via:

$$\rho(\xi,\eta,\tau) = \frac{\langle (f(x,y,t) f(x+\xi,y+\eta,t+\tau)\rangle}{\langle f^2(x,y,t)\rangle} \qquad \text{(A1)}$$

Based on the spatial and temporal evolution of the pattern, there is a family of surfaces in the (*ξ, η, τ*) plane – assumed to be ellipsoidal – that defines surfaces of constant correlation (the origin has $\rho = 1$, and the correlation strength decays in each direction away from the origin).

We define the coordinates (x', y', t') as those of a moving frame, stationary with respect to the overall drift of the pattern. In this frame, the correlation function will then be given by:

$$\rho(\xi',\eta',\tau') = \rho(A\xi'^2 + B\eta'^2 + 2H\xi'\eta' + K\tau^2) \qquad \text{(A2)}$$

Where *A, B, H,* and *K* are constants defining the shape of the pattern. The correlation function is constant at surfaces defining a tilted ellipse in the spatial dimensions (representing a generally anisotropic pattern), along with a term representing a decay in the time dimension.

If the pattern has bulk motion at speed V in the ϕ direction, a stationary observer's coordinates are defined relative to the moving observer by

$$x = x' + Vt\sin\phi = x' + V_x t \quad \text{(A3)}$$

$$y = y' + Vt\cos\phi = y' + V_y t \quad \text{(A4)}$$

Therefore, we substitute for ξ' and η' in Equation A2 to give

$$\rho(\xi,\eta,\tau) = \rho(A[\xi - V_x\tau]^2 + B\left[\eta - V_y\tau\right]^2 + 2H[\xi - V_x\tau]\left[\eta - V_y\tau\right] + K\tau^2)$$

Rearranging and combining terms, this becomes

$$\rho(\xi,\eta,\tau) = \rho(A\xi^2 + B\eta^2 + 2H\xi\eta + C\tau^2 + 2F\xi\tau + 2G\eta\tau + K\tau^2) \quad \text{(A5)}$$

Where we have defined F and G such that

$$F = -AV_x - HV_y \quad \text{(A6)}$$

$$G = -HV_x - BV_y \quad \text{(A7)}$$

These are equations (2) and (3) in the main body of the paper.
Now, in order to determine the velocity components V_x and V_y, we need to determine the coefficients of the ellipse *A, B, F, G,* and *H*, to within a multiplicative constant. This can be done by considering the following five time shifts obtained by cross- and auto-correlating the three signals obtained at S_0, S_1, and S_2:

1. τ_x: the time shift at which the auto-correlation matches the cross-correlation between signals S_0 and S_1 at zero lag. From Equation A5, the auto- correlation is given by

   $$\rho(\xi = 0, \eta = 0, \tau) = \rho(C\tau^2)$$

   The cross-correlation is given by

   $$\rho(\xi = \xi_0, \eta = 0, \tau = 0) = \rho(A{\xi_0}^2)$$

   For these to equate the arguments of the correlation functions must be equal, so we have

   $$\frac{A}{C} = \frac{\tau^2}{\xi_0^2} \quad \text{(A8)}$$

2. τ_y: the time shift at which the auto-correlation matches the cross-correlation between signals S_0 and S_2 at zero lag. Similarly,

   $$\frac{B}{C} = \frac{\tau_y^2}{\eta_0^2} \quad \text{(A9)}$$

3. τ_{xy}: the time shift at which the auto-correlation matches the cross-correlation between signals S_1 and S_2. Here, equating the arguments gives

$$\frac{H}{C} = \frac{\tau_{xy}^2}{2\xi_0\eta_0} = \frac{A\xi_0}{2C\eta_o} - \frac{B\eta_0}{2C\xi_0} \qquad \text{(A10)}$$

Since *A/C* and *B/C* have already been found, this is sufficient to obtain *H/C*

4. τ'_x: the time shift at which the correlation between signals S_0 and S_1 is maximized. Equation A5 becomes

$$\rho(\xi = \xi_0, \eta = 0, \tau) = \rho(A\xi_0^2 + 2F\xi_0\tau + C\tau^2)$$

For the maximal time shift τ'_x we must have

$$\frac{\partial\rho}{\partial\tau} = (2F\xi_0 + 2C\tau'_x)\rho' = 0$$

And so we obtain

$$\frac{F}{C} = -\frac{\tau'_x}{\xi_0} \qquad \text{(A11)}$$

5. τ'_y: the time shift at which the correlation between signals S_0 and S_1 is maximized. Similarly,

$$\frac{G}{C} = -\frac{\tau'_y}{\eta_0} \qquad \text{(A12)}$$

By substituting equations A8, A9, A10, A11 and A12 into equations A6 and A7 and solving the system of equations, the x- and y- components of the bulk drift velocity, V_x and V_y are then obtained.